Selective non-oxidative dehydrogenation of ethanol to acetaldehyde and hydrogen on highly dilute NiCu alloys

Junjun Shan [a,1], Nare Janvelyan [b,1], Hang Li [a], Jilei Liu [a], Tobias M. Egle [c], Jianchao Ye [c], Monika M. Biener [c], Juergen Biener [c], Cynthia M. Friend [b], Maria Flytzani-Stephanopoulos [a,*]

[a] Department of Chemical and Biological Engineering, Tufts University, Medford, MA 02155, USA
[b] Department of Chemistry and Chemical Biology, Harvard University, Cambridge, MA 02138, USA
[c] Nanoscale Synthesis and Characterization Laboratory, Lawrence Livermore National Laboratory, Livermore, CA 94550, USA

ARTICLE INFO

ABSTRACT

The non-oxidative dehydrogenation of ethanol to acetaldehyde has long been considered as an important method to produce acetaldehyde and clean hydrogen gas. Although monometallic Cu nanoparticles have high activity in the non-oxidative dehydrogenation of ethanol, they quickly deactivate due to sintering of Cu. Herein, we show that adding a small amount of Ni ($Ni_{0.01}Cu - Ni_{0.001}Cu$) into Cu to form highly dilute NiCu alloys dramatically increases the catalytic activity and increases their long-term stability. The kinetic studies show that the apparent activation energy decreases from ∼70 kJ/mol over Cu to ∼45 kJ/mol over the dilute NiCu alloys. The improved performance is observed both for nanoparticles and nanoporous NiCu alloys. The improvement in the long-term stability of the catalysts is attributed to the stabilization of Cu against sintering. Our characterization data show that Ni is atomically dispersed in Cu. The comparison of the catalytic performance of highly dilute alloy nanoparticles with nanoporous materials is useful to guide the design of novel mesoporous catalyst architectures for selective dehydrogenation reactions.

© 2017 Elsevier B.V. All rights reserved.

1. Introduction

Acetaldehyde (CH_3CHO) is an important commodity chemical and is widely used as the starting material for the synthesis of a large number of industrial chemicals such as acetic acid, acetate esters, and pentaerythritol [1,2]. The selective non-oxidative dehydrogenation (DH) of ethanol to acetaldehyde and hydrogen is an important industrial reaction to produce acetaldehyde [3,4]. It is also an essential first step in ethanol steam reforming and ethanol partial oxidation reactions [5,6]. Monometallic Cu-based catalysts are widely used for this reaction; however, quick deactivation of copper takes place, attributed to copper particle sintering [4,7]. On the other hand, the oxidative dehydrogenation (ODH) of ethanol to acetaldehyde and water is the oldest laboratory method to produce acetaldehyde. Commercially, ODH is typically catalyzed by copper, silver, and their oxides or alloys with air in the vapor phase. [1]. Sim-

ilar to the case of DH, the fast deactivation of the catalysts remains a challenging problem [8,9]. Since DH also produces hydrogen, another valuable product, it is attractive to develop new catalysts that are highly active and selective, with improved catalyst stability during the ethanol dehydrogenation reaction. Naturally, the first consideration is the development of Cu-based alloys possessing these properties.

Although supported Cu based catalysts have been extensively studied for the ethanol dehydrogenation reaction, there is still disagreement on the chemical state of the active Cu species during the reaction. Several groups have reported that Cu^+ is the most active species [10–12], while other studies find that high dehydrogenation activity is associated with the presence of metallic Cu [13,14]. On the other hand, as mentioned above, the catalytic activity of Cu has been found to decrease rapidly even in the first hour of the reaction, where the deactivation has been attributed to the sintering of metallic Cu at the high dehydrogenation temperature [7,14]. In searching for a promoter to inhibit the sintering of Cu, it has been reported that the incorporation of chromium oxide into Cu improves the catalyst stability [13,15,16]. However, the adverse environmental issues associated with the use of chromium have discouraged the application of this approach. The addition of alkali

metal oxides has also been reported to improve the stability of Cu, although the effect is less significant than chromium oxide [7].

Alternatively, the dehydrogenation of ethanol on Au NPs supported on reducible oxides has also been explored [3,17–19]. Supported Au NPs with certain particle sizes have been demonstrated to have high activity and selectivity for the reaction [3]. An exception is Au/Al₂O₃, where the dehydration of ethanol to ethylene and dimethyl ether dominates the reaction [18]. Recently, Wang et al. have reported that isolated Au species supported on nanoscale ZnZrOₓ composite oxides catalyze the dehydrogenation of ethanol to acetaldehyde and hydrogen with 100% selectivity at low temperatures (~200 °C), even in the presence of water, in a well-separated temperature window from the dehydration and steam reforming reactions that take place on the support [17]. The presence of atomically dispersed Au species seems to play an essential role in the activation of ethanol and its subsequent dehydrogenation reaction.

In recent years, development of catalysts with atomic dispersions of an active metal on various supports has attracted considerable attention [20]. In the case of bimetallic catalysts, various highly dispersed alloys or even single atom alloy (SAA) catalysts containing atomically dispersed active species have been reported to be highly active and selective for many catalytic reactions. For example, atomically dispersed Au species supported on ZnZrOₓ oxides catalyze the ethanol dehydrogenation reaction, as discussed above [17]. Isolated Pt and Au cations stabilized by −O bonds on various supports supplying vicinal −OH groups have been found to be highly active for the water-gas shift reaction [21–24]. PdAu bimetallics have been reported as selective hydrogenation catalysts in both gas-phase[25–27] and liquid-phase reactions [28,29]. These studies have focused on bimetallic nanoparticles supported on carbon, oxides or other supports. It has also been reported that unsupported gold, prepared in nanoporous form from AuAg alloys after leaching out most (~97%) of the silver, is an effective catalyst for the selective oxidation of methanol, and other alcohols [30,31]. Since unsupported gold is inert, it was apparent that the active sites must be at the interface of silver domains and gold. These sites also catalyze the oxidative self-coupling of methanol to methyl formate[32] and the cross coupling of methanol with higher alcohols or aldehydes to form esters [33]. The interaction of gold with nickel in Au@NiOₓ core-shell nanoparticles rather than silver has been exploited by Asahi Chemicals recently to selectively oxidize methacrolein with methanol to produce methyl methacrylate (MMA) in industrial volumes [34].

Similar to gold, copper is a highly selective hydrogenation metal, but it has negligible activity for the hydrogenation of alkadienes or alkynes, limited by a large activation energy barrier for dissociative adsorption of hydrogen [35]. However, it was recently shown that adding Pd or Pt atoms to metallic Cu hosts forming PdCu or PtCu SAAs is a good strategy to produce truly bi-functional catalysts, whereby the Pd or Pt atom dissociates H₂ and spills over H atoms to the Cu surface, rendering the latter active for alkyne and alkadiene hydrogenation reactions [36–38]. The SAAs have superior selectivity to the Pt or Pd monometallics. Excellent selectivity for dehydrogenation of methanol has also been demonstrated on PdCu and PtCu SAAs, the Pd or Pt atoms serve as exit points for the association of H atoms and desorption of H₂ [39,40].

In the present study, we have investigated the addition of Ni in Cu as a novel catalyst for the selective dehydrogenation of ethanol to acetaldehyde and hydrogen. Ni-containing Cu nanoparticles (NiCu NPs) and nanoporous Cu (np-NiCu) materials were prepared with high dispersions of Ni in Cu and found to be very active and selective for this reaction. The presence of atomically dispersed Ni in Cu dramatically decreases the apparent activation energy from ~70 kJ/mol over Cu to ~45 kJ/mol over NiCu alloys. Moreover, Ni efficiently suppresses the coarsening of Cu during the

dehydrogenation reaction, thus increasing the long-term stability of these catalysts.
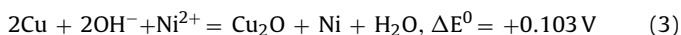
2. Experimental

2.1. Catalyst preparation

In this work, several types of highly dilute NiCu alloys were prepared as supported nanoparticles and unsupported nanoporous alloys. These were silica supported NiCu NPs, unsupported nanoporous NiCu prepared through a sacrificial support method labeled np-NiCu (SSM), and nanoporous NiCu prepared through a dealloying technique labeled np-NiCu (DL). Silica supported NiCu NPs with various Ni concentrations were synthesized through a wet chemistry method followed by a modified electroless galvanic deposition method. In the first step, metallic Cu nanoparticles were prepared as colloids in solution as described in detail in our recent publications [38,40]. Briefly, under nitrogen protection, a 0.1 M solution of ascorbic acid was added to a mixed aqueous solution of Cu(NO₃)₂ and polyvinylpyrrolidone (PVP) (200:1 molar ratio of Cu to PVP), followed by drop-wise addition of NaBH₄ (0.1 M), upon which the solution turned to an opaque brown suspension. Fumed silica, with a surface area of 200 m²/g (as received), was pre-activated by heating in air at 650 °C for 12 h, suspended in deionized water under constant stirring, and added drop-wise to the colloidal solution. The solution was kept under nitrogen protection and constant stirring for 30 min, followed by filtering and washing with deionized water several times. The collected solid was dried in vacuum for 12 h and calcined in air to 350 °C for 4 h. The product was subsequently reduced in pure hydrogen at 350 °C for 3 h to obtain supported metallic Cu NPs. The typical Cu loading is 8 wt% as determined by inductively coupled plasma (ICP) elemental analysis.

In our previous studies, galvanic replacement (GR) has been successfully used to prepare PdCu and PtCu single atom alloys [37,38]. However, GR is not an applicable method to deposit Ni to Cu surface, since Ni has a lower reduction potential (Ni²⁺/Ni, E⁰ = −0.257 V) than Cu (Cu²⁺/Cu, E⁰ = +0.340) [41]. Therefore, a novel modified electroless galvanic deposition method was developed to deposit highly dispersed Ni to the Cu NPs. The following redox reactions show the principle of this method:

$$Ni^{2+} + 2e^- = Ni, E^0 = -0.257\,V \tag{1}$$

$$Cu_2O + H_2O + 2e^- = 2Cu + 2OH^-, E^0 = -0.360\,V \tag{2}$$
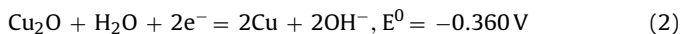
Combination of (1) and (2) gives:

$$2Cu + 2OH^- + Ni^{2+} = Cu_2O + Ni + H_2O, \Delta E^0 = +0.103\,V \tag{3}$$

Reaction (3) is spontaneous; accordingly, Ni atoms are deposited on the surface of Cu₂O, which is formed by the oxidation of the Cu metal in the presence of OH⁻ (alkaline solution). The deposition was as follows: first, a certain amount of Ni(NO₃)₂·6H₂O was completely dissolved in deionized water under nitrogen bubbling and continuous stirring. Then, 0.01 M NaOH was added drop-wise to the solution to reach a pH value of 10.83. The desired amount of pre-reduced silica-supported Cu NPs was then added into the solution. The reaction was held for 1 h under nitrogen protection and continuous stirring. The typical atomic ratio of Ni to Cu ranged from 1:100 to 1:1000. Subsequently, the suspension was filtered and washed with deionized water several times, followed by vacuum drying at 70 °C for 12 h. The obtained solid was further reduced in pure hydrogen at 400 °C for 3 h. The Ni loading was measured by ICP.

We also prepared np-NiCu (SSM) catalysts through the sacrificial support method [42]. To do this, pre-reduced Cu/SiO₂ powder was dispersed in an 8 M KOH solution under continuous stirring at room temperature. This leaching process continued for 36 h to

ensure that the majority of the silica support was leached away. In this process, the color of the solution changed from dark-brown initially to red-brown at the end. The solid was filtered and washed with deionized water until the pH value of the filtrate was neutral, followed by vacuum drying at 70 °C for 12 h. The obtained materials were then reduced in pure hydrogen at 350 °C for 3 h to obtain np-Cu (SSM). Ni was introduced to the surface of np-Cu (SSM) using the galvanic deposition method discussed above. After Ni deposition, the solid was reduced in pure hydrogen at 400 °C for 3 h to obtain the final product np-NiCu (SSM). The atomic ratio of Ni to Cu in np-NiCu (SSM) catalysts was determined by ICP measurements.

Alternatively, np-NiCu (DL) was prepared through dealloying of Cu-Zn alloys followed by a liquid salt impregnation/freeze drying Ni addition process. Firstly, np-Cu (DL) ingots were prepared by the selective etching the Zn from $Cu_{50}Zn_{50}$ bimetallic alloy disks in 5 M hydrochloric acid for 36 h. The resulting nanoporous Cu sample was rinsed with deionized water and dried in a vacuum oven, labeled as np-Cu (DL). To prepare np-NiCu (DL), part of np-Cu (DL) was immersed in nickel(II) nitrate solution with a nickel concentration of 0.3 M. To guarantee full penetration of solution into the pores of np-Cu (DL), vacuum was applied for 2 h to remove air bubbles trapped inside the core of np-Cu (DL). The sample was then kept under atmospheric conditions in solution overnight, followed by a freeze-drying precursor method, in which the sample was immersed into liquid nitrogen for 10 min and subsequently kept in a freeze-drying system at 0.012 mbar and −106 °C (Labconco, FreeZone 4.5 l Benchtop Freeze Dry System) for 2 days. Freeze drying helps to keep the homogeneous distribution of Ni precursors while removing water [43], therefore, it allows a high dispersion of Ni in Cu after drying. In the final step, the sample was reduced in hydrogen (4% H_2 balanced in Ar) at 500 °C for 1 h. The atomic ratio of Ni to Cu in the np-NiCu (DL) material was determined as approximately 0.03:1 through ICP measurements. ICP also found approximately 4% Zn residue in the np-Cu (DL) and np-NiCu (DL) materials.

2.2. Characterization techniques

X-ray powder diffraction (XRD) patterns were collected on a PANalytical X'Pert Pro instrument using nickel-filtered Cu Kα radiation (λ = 1.54056 Å). The measurements were taken at 45 kV and 40 mA in a continuous mode. Data was collected for 2θ between 25° and 80°. High-resolution transmission electron microscope (HRTEM) images of highly dilute NiCu alloys were obtained with a JEOL 2100 TEM system. All samples for HRTEM characterization were prepared by dropping the corresponding colloidal solutions onto lacey carbon TEM grids. Scanning electron microscope (SEM) images were taken using a Zeiss Supra 55VP microscope.

X-ray photoelectron spectroscopy (XPS) characterization was performed with a PHI VersaProbe II system equipped with a monochromatic Al Kα source and a double focusing hemispherical analyzer. The XPS system is also equipped with an argon ion sputter gun for depth-profile analysis. XPS samples were prepared by loading the catalyst powder onto a Cu foil. XPS data were analyzed using the Casa XPS software. Diffuse reflectance infrared Fourier transform spectroscopy (DRIFTS) measurements were performed on a Thermo Scientific Nicolet iS50 FTIR Spectrometer and a Praying Mantis high temperature reaction chamber. NiCu alloys were reduced in situ with 10% H_2/He at a flow rate of 10 mL/min at 350 °C for 1 h. CO adsorption on the NiCu samples was performed at room temperature. Pure CO was introduced into the DRIFTS cell at a flow rate of 10 mL/min. This was followed by a He purge at a flow rate of 20 mL/min to remove gas phase CO in the cell prior to DRIFTS measurements.

The ethanol dehydrogenation activity of the NiCu alloys was evaluated in a fixed-bed flow reactor at atmospheric pressure. Typ-
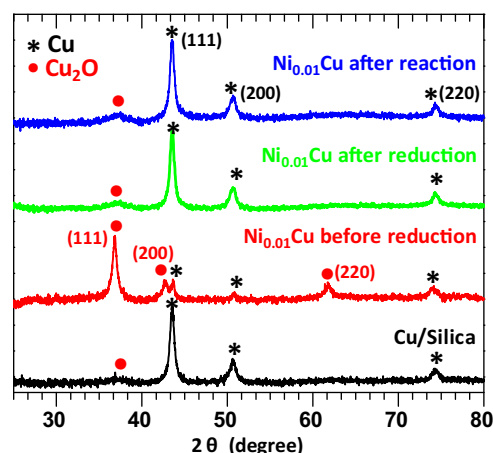

Fig. 1. XRD patterns of silica supported Cu NPs and silica supported $Ni_{0.01}$Cu NPs before reduction, after reduction, and after the ethanol dehydrogenation reaction at 250 °C for 8 h.

ically 100 mg sample was loaded into a U-shaped quartz reactor tube between two layers of quartz sand and packed in between two quartz wool plugs. The reactor was heated in a furnace equipped with a temperature controller. The temperature of the catalyst was measured with a K-type thermocouple reaching the top of the catalyst bed. Prior to testing, all catalysts were reduced under a flow of H_2 (10% in argon) with a flow rate of 10 mL/min at 350 °C for 1 h. The typical reaction gas composition was 5.6% ethanol balanced in He, through a bubbler system, using a flow rate of 10 mL/min. The effluent gas was monitored online by a residual gas analyzer (SRS RGA 200). Ethanol, acetaldehyde, ethyl acetate, H_2, CO, CO_2, and C_2H_4 were monitored by m/z = 31, 29, 61, 2, 28, 44, and 27, respectively. In addition, in the case of acetaldehyde, the contribution from the ethanol fragment was subtracted from the original m/z = 29 signal prior to further processing.

Long-term ethanol dehydrogenation activity was tested in a quartz tube reactor operated at atmospheric pressure and housed in a tubular furnace. Hydrogen treatment was performed in 20% H_2 with a flow rate of 20 mL/min. The temperature was ramped to 250 °C for Cu catalysts and 350 °C for NiCu catalysts at a rate of 10 °C/min and held for 1 h. The sample was held or cooled to 250 °C after hydrogen treatment and then exposed to reaction conditions of 5.6% ethanol using a flow rate of 7.5 mL/min. To provide ethanol, He gas was flowed through a bubbler filled with liquid ethanol held at room temperature. The effluent gas was continuously analyzed by a GC–MS (Agilent 5975C and Agilent 7890A) equipped with HP-PLOT Q and CARBONPLOT columns.

3. Results and discussion

Inspired by our recent findings of methanol dehydrogenation on PtCu single atom alloy catalysts [40], we prepared highly dilute NiCu alloy catalysts and examined their catalytic performance in the selective ethanol dehydrogenation reaction under realistic reaction conditions. As discussed below, Ni is atomically dispersed in Cu in the selective catalysts. Our work demonstrates that such Ni species play a key role in the dehydrogenation of ethanol.

XRD patterns of silica supported Cu NPs, silica supported $Ni_{0.01}$Cu NPs before reduction, silica supported $Ni_{0.01}$Cu NPs after reduction, and silica supported $Ni_{0.01}$Cu NPs after use in ethanol dehydrogenation at 250 °C for 8 h are shown in Fig. 1. The XRD pattern of Cu NPs is dominated by diffraction peaks that are attributed to the (111), (200) and (220) lattice planes of metallic Cu [44]. A rather broad peak centered at 37° can be attributed to the (111) diffraction of Cu_2O [44]. The appearance of a small Cu_2O diffrac-
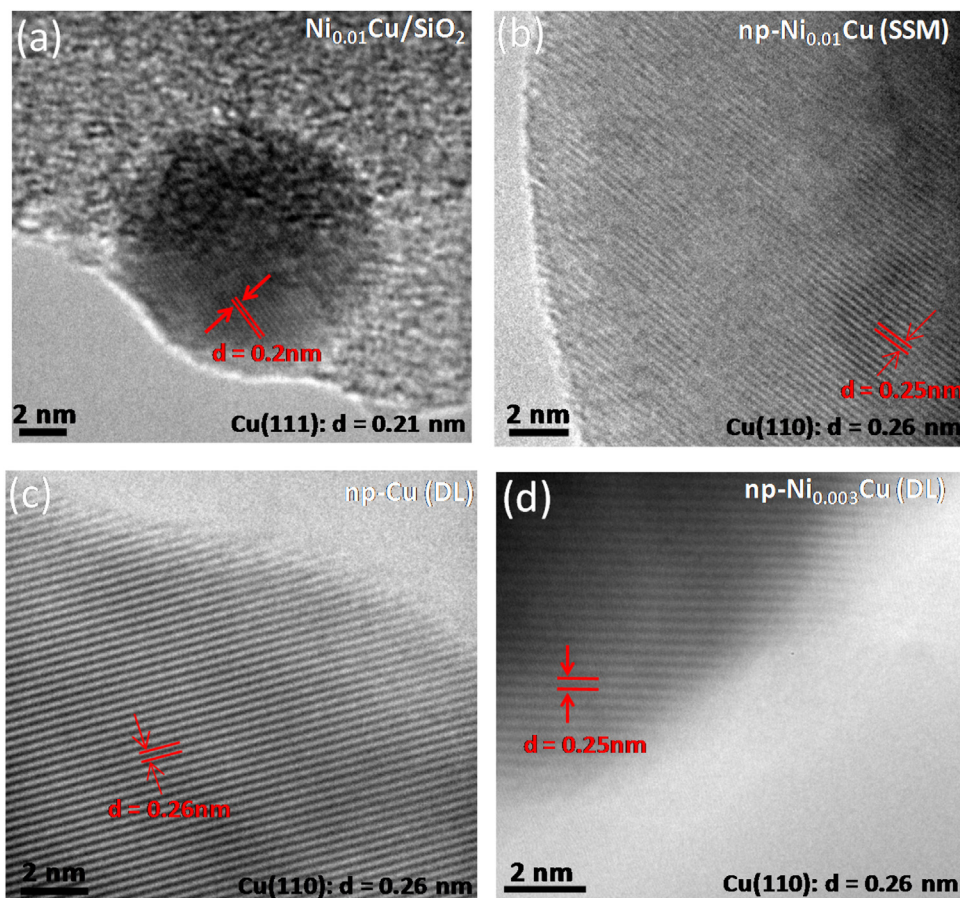
Fig. 2. (a) HRTEM image of a silica supported $Ni_{0.01}Cu$ nanoparticle; (b) HRTEM image of a typical region of the np-$Ni_{0.01}Cu$ (SSM) catalyst; (c) HRTEM image of np-Cu (DL); (d) HRTEM image of np-$Ni_{0.003}Cu$ (DL). All samples were imaged in their as-prepared form.

tion peak is due to the formation of a thin Cu_2O surface layer after the exposure of metallic Cu NPs to air [44,45]. For $Ni_{0.01}Cu$ before reduction, the XRD pattern clearly shows that Cu_2O is the majority phase, which is expected because of the oxidation of Cu to Cu_2O by OH^- during the Ni deposition step. After reduction, Cu_2O was reduced and metallic Cu peaks are dominant. Moreover, XRD patterns of $Ni_{0.01}Cu$ NPs after reduction show no observable difference compared to Cu NPs, as expected if Ni is atomically dispersed, and mostly on the near surface layer of Cu (see XPS data below). No Ni NPs related XRD peaks are observed, although the Ni concentration in $Ni_{0.01}Cu$ NPs is probably too low to exclude the formation of Ni NPs based on the XRD data alone. Similarly, the XRD patterns of $Ni_{0.01}Cu$ after the reaction were preserved, and no separate Ni phases were formed, at least not detectable by XRD at these small Ni content. In all samples, the estimated average crystallite size of Cu is ∼14 nm, as calculated by the Scherrer equation.

Fig. 2 shows HRTEM images of NiCu alloys. Fig. 2a shows the image of silica supported $Ni_{0.01}Cu$ NPs. The lattice fringes of $Ni_{0.01}Cu$ NPs show a spacing of 0.2 nm, in good agreement with the [111] lattice planes of Cu [46]. Moreover, the measured nanoparticle size is ∼13–14 nm, in good agreement with the XRD analysis of Fig. 1. The HRTEM images in Fig. 2b, 2c and 2d clearly exhibit the crystalline nature of nanoporous materials, indicating that the nanoporous NiCu alloys prepared by either the sacrificial support method or the dealloying method are not amorphous but are well-crystallized. Furthermore, the HRTEM images collected from np-$Ni_{0.01}Cu$ (SSM), np-Cu (DL), and np-$Ni_{0.003}Cu$ (DL) samples all show the (110) lattice fringes of metallic Cu (lattice spacing 0.25 nm) [47]. Unfortunately, due to the similar atomic number of

Table 1
Cu surface area of silica supported $Ni_{0.01}Cu$ NPs, np-$Ni_{0.01}Cu$ (SSM), and np-$Ni_{0.003}Cu$ (DL).

Samples	Surface area of Cu (m²/g)
$Ni_{0.01}Cu$ NPs	48
np-$Ni_{0.01}Cu$ (SSM)	8.7
np-$Ni_{0.003}Cu$ (DL)	2.7

Ni and Cu, it is impossible to distinguish Ni from Cu through Z-contrast imaging in scanning TEM measurements [48]. Indeed, Ni species cannot be distinguished by TEM in the highly dilute NiCu alloys of Fig. 2.

SEM images of np-$Ni_{0.01}Cu$ (SSM) and np-$Ni_{0.003}Cu$ (DL), after reduction in hydrogen (10% balanced in Ar) at 350 °C for 1 h, as well as np-Cu (DL) after reduction in hydrogen (10% balanced in Ar) at 250 °C for 1 h, are shown in Fig. 3. They illustrate the porous structure of these nanoporous materials. Clearly, these highly dilute NiCu alloys prepared by the sacrificial support method or by dealloying are porous materials with well-crystallized nanostructure. The average feature size of np-$Ni_{0.01}Cu$ (SSM) is 395 ± 99 nm, whereas for np-Cu (DL) and np-$Ni_{0.003}Cu$ (DL) they are 150 ± 35 and 209 ± 41 nm, respectively. The average feature size of np-$Ni_{0.003}Cu$ is larger than that of np-Cu, which we attribute to the additional reduction step at 500 °C for np-$Ni_{0.003}Cu$ during the step of synthesis.

Table 1 lists the specific surface areas (per gram of Cu) of silica supported $Ni_{0.01}Cu$ NPs, np-$Ni_{0.01}Cu$ (SSM), and np-$Ni_{0.003}Cu$ (DL). The surface area of silica supported $Ni_{0.01}Cu$ NPs was calcu-
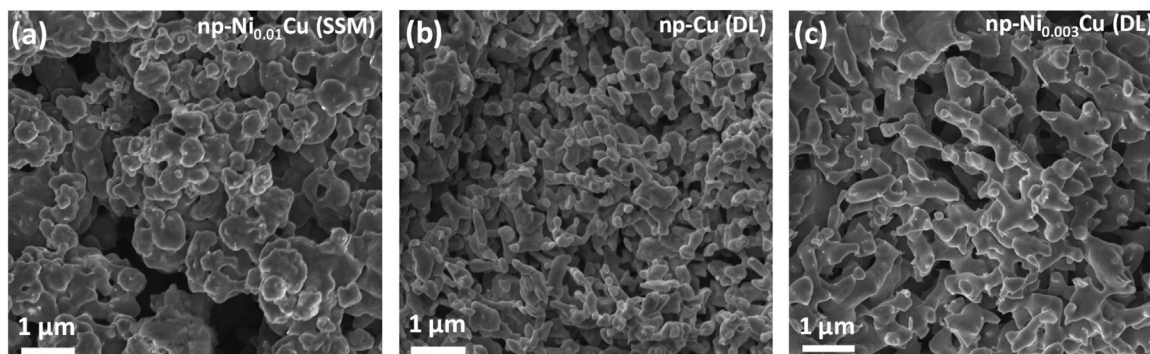
Fig. 3. (a) SEM image of np-$Ni_{0.01}Cu$ (SSM); (b) SEM image of np-Cu (DL); (c) SEM image of np-$Ni_{0.003}Cu$ (DL). np-$Ni_{0.01}Cu$ (SSM) and np-$Ni_{0.003}Cu$ (DL) were pre-reduced in hydrogen (10% balanced in Ar) at 350 °C for 1 h prior to SEM imaging, while np-Cu (DL) was pre-reduced at 250 °C for 1 h prior to SEM imaging.
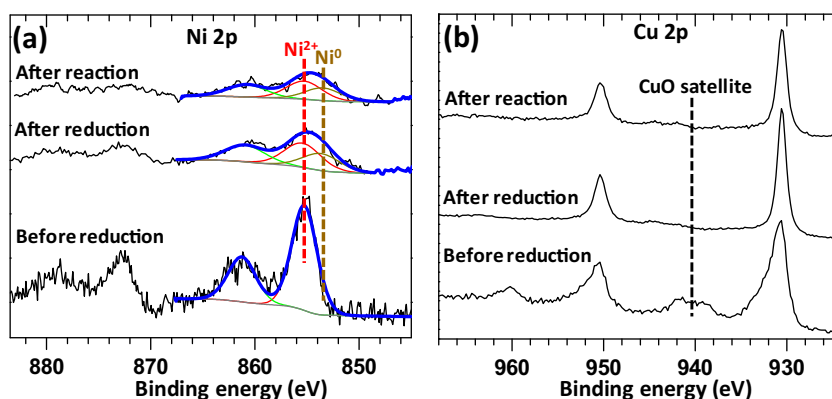

Fig. 4. The photoemission feature of Ni 2p (a) and Cu 2p (b) of np-$Ni_{0.01}Cu$ (SSM) before reduction, after reduction, and after the ethanol dehydrogenation reaction at 250 °C for 8 h. Approximately 10 consecutive scans were collected for the sample before reaction, and approximately 40 consecutive scans were collected for the samples after reduction and after reaction.

lated based on following equations, assuming the spherical shape of particles: [7,49]

$$S_{Cu}(m^2/g) = 6.73 \times 10^{11}/d_{Cu}(nm) \qquad (4)$$

where S_{Cu} is the specific surface area of Cu (m^2/g), while d_{Cu} stands for the average particle size of Cu (nm), here ~14 nm as determined from XRD and TEM. The surface areas of np-$Ni_{0.01}Cu$ (SSM) and np-$Ni_{0.003}Cu$ (DL) were determined from BET measurements, listed in Table 1. The silica supported nanoparticles, $Ni_{0.01}Cu$ NPs, have the largest specific copper surface area among these catalysts.

Fig. 4a and b shows the photoemission features of Ni 2p and Cu 2p of np-$Ni_{0.01}Cu$ (SSM) before reduction, after reduction, and after the ethanol dehydrogenation reaction at 250 °C for 8 h. Table 2 lists the surface atomic ratio of Ni/Cu estimated from XPS. The surface Ni/Cu atomic ratio before reduction is 0.12 and decreases to 0.06 after reduction, a value that persists after the ethanol dehydrogenation reaction, suggesting that after reduction in hydrogen atmosphere part of Ni atoms diffuse to the subsurface, and remain in the subsurface during the ethanol dehydrogenation reaction. Furthermore, Ni 2p photoemission spectra also indicate that before reduction Ni^{2+} is the dominant species [50,51]. It has been reported that highly dispersed metallic Ni can be easily oxidized to NiO under atmospheric conditions [52,53]. Whilst after reduction, the peak related to the metallic Ni significantly grows [50,51]. The remaining of Ni^{2+} after reduction is possibly due to the fact that NiO was not fully reduced at 400 °C, while it could also result from the re-oxidation of Ni^0 after exposing the sample to air after reduction. On the other hand, Cu 2p photoemission spectra show that before reduction the features centered at 940 and 962 eV are present, while they disappear after reduction and after reaction; these fea-

tures are assigned to the satellite peaks of CuO [54]. Clearly, Cu^{2+} is only present in np-$Ni_{0.01}Cu$ (SSM) before reduction, not in np-$Ni_{0.01}Cu$ (SSM) after reduction and after reaction. On the other hand, Cu_2O does not have satellite peaks in XPS, and also the main peak of Cu^{1+} is overlapped with metallic Cu. Therefore XPS data in Fig. 4 cannot distinguish Cu_2O from metallic Cu. Furthermore, we also tried to obtain Ni 2p photoemission features of silica supported $Ni_{0.01}Cu$ NPs, however the low Ni concentration in the supported catalyst does not yield a measurable signal of Ni. Moreover, we also took the Ni 2p photoemission spectra of np-$Ni_{0.003}Cu$ (DL) (not shown here); the spectra are similar to np-$Ni_{0.01}Cu$ (SSM), and the surface atomic ratio of Ni/Cu is shown in Table 2. Similar to np-$Ni_{0.01}Cu$ (SSM), the surface Ni/Cu ratio of np-$Ni_{0.003}Cu$ (DL) suggests that after reduction, part of Ni atoms diffuse to the subsurface, and remain there during the reaction.

Using CO as a probe molecule, DRIFT spectra were collected on silica supported Cu NPs, Fig. 5a, and silica supported $Ni_{0.01}Cu$ NPs, Fig. 5b, at various temperatures. All samples were reduced in situ in 10% H_2 (balanced in He) at 350 °C for 1 h prior to the introduction of CO. The adsorption of CO was performed at room temperature with a flow rate of 10 mL/min followed by a He purge at a flow rate of 20 mL/min for 10 min. Prior to acquiring the DRIFTS data, samples were heated to the desired temperature in He for 10 min and maintained at this temperature during the data acquisition. CO-DRIFT spectra in Fig. 5a show a single peak centered at approximately 2128 cm^{-1}, which may be attributed to either the Cu^+–CO carbonyl species or the atop binding of CO on Cu NPs [36,55]. With increasing temperatures, the peak area continuously decreases, indicating desorption of CO from the Cu surface. Clearly, at 100 °C, this peak

Table 2
The surface atomic ratio of Ni/Cu of np-$Ni_{0.01}$Cu (SSM) and np-$Ni_{0.003}$Cu (DL) under various conditions.

Sample conditions	Surface Ni/Cu ratio of np-$Ni_{0.01}$Cu (SSM)	Surface Ni/Cu ratio of np-$Ni_{0.003}$Cu (DL)
Before reduction	0.12	0.035
After reduction at 400 °C	0.06	0.013
After reaction at 250 °C	0.06	0.013
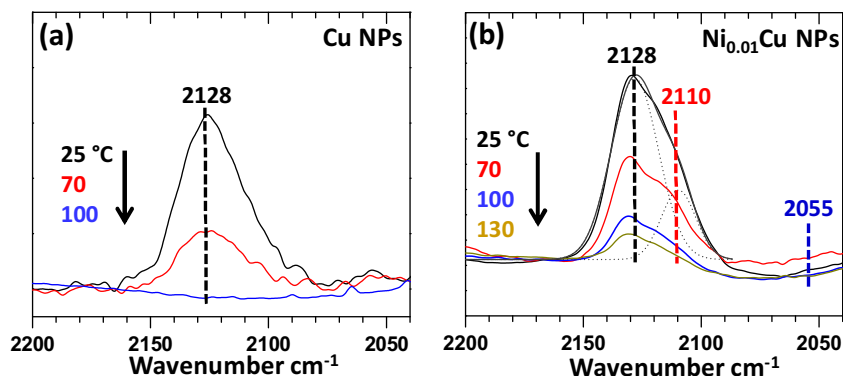
Fig. 5. CO-DRIFT spectra of silica supported Cu NPs (a), and silica supported $Ni_{0.01}$Cu NPs (b), at various temperatures. All samples were reduced in situ at 350 °C in hydrogen (10% balanced in He) for 1 h. The CO adsorption was performed at room temperature with a flow rate of 10 mL/min followed by a He purge with a flow rate of 20 mL/min for 10 min prior to DRIFTS measurements.

disappears completely, suggesting that all the CO species had desorbed.

On the other hand, DRIFT spectra on the supported $Ni_{0.01}$Cu NPs, Fig. 5b, show an additional shoulder at 2110 cm^{-1} besides the 2128 cm^{-1} peak. Similar to Fig. 5a, the 2128 cm^{-1} peak is assigned to CO binding to Cu surface atoms, while the additional 2110 cm^{-1} peak must be related to the presence of Ni surface atoms. Indeed, the 2110 cm^{-1} peak can be attributed to $Ni(CO)_x$ sub-carbonyl species with x = 2 or 3 [56]. The formation of such sub-carbonyl species indicates a high dispersion of Ni species [56,57]. Furthermore, the linear CO absorption band on Ni NPs is reported at 2055 cm^{-1} [56], which is completely absent in Fig. 5b, indicating that the presence of metallic nickel nanoparticles can be excluded. Moreover, the adsorption bands related to CO on Ni^{2+}/Ni^{1+} species are usually reported in the region of 2190–2200 cm^{-1} [58], which are not present in the spectra of $Ni_{0.01}$Cu NPs. Therefore, the DRIFTS measurements suggest the presence of neutral atomic Ni species in $Ni_{0.01}$Cu NPs. In addition, the Ni related signal at 2110 cm^{-1} is relatively strong given the low Ni surface concentration determined by XPS, thus indicating preferential CO adsorption at Ni sites. On the other hand, the relatively small concentration of Ni in $Ni_{0.001}$Cu NPs does not allow us to obtain reasonable Ni sub-carbonyl signal at 2110 cm^{-1} in DRIFTS measurements; however, it is expected that Ni is atomically dispersed in Cu in the case of $Ni_{0.001}$Cu NPs.

Interestingly, Fig. 5b also shows that although the peak area of 2128 cm^{-1} feature decreases with increasing temperatures, the decreasing rate is much smaller than the rate on the bare Cu NPs. For example, at 100 °C, Fig. 5a shows that all the CO species were desorbed from the Cu NPs, whereas Fig. 5b shows that even at 130 °C, the CO species adsorbed on Cu are still clearly present. Therefore, surprisingly, addition of a small amount of Ni to Cu can strengthen the binding of CO on the Cu surface.

The catalysis tests were first performed over silica supported NiCu NPs with different Ni concentrations. Fig. 6 shows the temperature-programmed surface reaction (TPSR) of ethanol (6% balanced in He) on silica supported $Ni_{0.001}$Cu NPs, $Ni_{0.01}$Cu NPs, and $Ni_{0.03}$Cu NPs with a heating rate of 10 °C/min. In all cases, formation of hydrogen and acetaldehyde is clearly observed, indicating the occurrence of ethanol dehydrogenation reaction. Because our mass spectrometer is connected to the reaction cell through a rela-

tively long cold stainless steel tube, the signal of ethanol is delayed compared to the signals of other gaseous products. Therefore, the drop of ethanol signal is out of the temperature windows shown in Fig. 6. Note that, the expected drop in the ethanol signal is observed when a lower heating rate is used. However, the ratio of acetaldehyde to H_2 is 1:1 when no CO or CO_2 is produced, and mass balance calculations in all cases show carbon closure close to 100%. For $Ni_{0.001}$Cu NPs and $Ni_{0.01}$Cu NPs, the formation of CO and CO_2 is negligible up to 350 °C, indicating a nearly 100% selectivity to acetaldehyde, which is similar to the observation on Cu NPs (not shown here). On $Ni_{0.03}$Cu NPs, formation of CO is observed even at a low temperature, thus indicating to the partial decomposition of ethanol to H_2 and CO along with the dehydrogenation reaction. It has been reported that Ni NPs are active for the ethanol dehydrogenation reaction with CO and H_2 being the dominant products, particularly at temperatures >300 °C [59]. Therefore, the TPSR data suggests that for the case of $Ni_{0.03}$Cu NPs, the formation of CO is likely resulting from the presence of relatively large Ni clusters, such as linear chains of Ni. The formation of Pt linear chains on Cu(111) surface has been observed and found to be active for C—C bond scission [37]. Similar to Pt, the larger Ni ensembles within the Cu matrix are likely capable of breaking C—C bonds leading to the formation of CO. While for $Ni_{0.001}$Cu and $Ni_{0.01}$Cu NPs, the presence of large Ni clusters seem to be negligible, in other words, Ni is highly or even atomically dispersed in Cu. This observation is consistent with the DRIFTS data discussed above. Furthermore, ethanol TPSR measurements on np-$Ni_{0.003}$Cu (DL) and np-$Ni_{0.01}$Cu (SSM) catalysts were also performed (not shown here). TPSR data show that these nanoporous catalysts exhibit a similar selectivity as supported $Ni_{0.001}$Cu and $Ni_{0.01}$Cu NPs, i.e. the only products are acetaldehyde and H_2.

Kinetic studies of the ethanol dehydrogenation reaction on various NiCu alloys were performed by measuring the reaction rate at various temperatures under steady-state conditions. In all measurements, the conversion of ethanol was kept below 15%. Fig. 7 shows an Arrhenius-type plot of the H_2 formation rate on the silica supported monometallic Cu NPs, $Ni_{0.001}$Cu NPs, $Ni_{0.01}$Cu NPs, np-Cu (SSM), np-$Ni_{0.01}$Cu (SSM), as well as np-$Ni_{0.003}$Cu (DL). The H_2 formation rates are normalized by the Cu surface area of each catalyst. The calculated apparent activation energies from the Arrhenius-
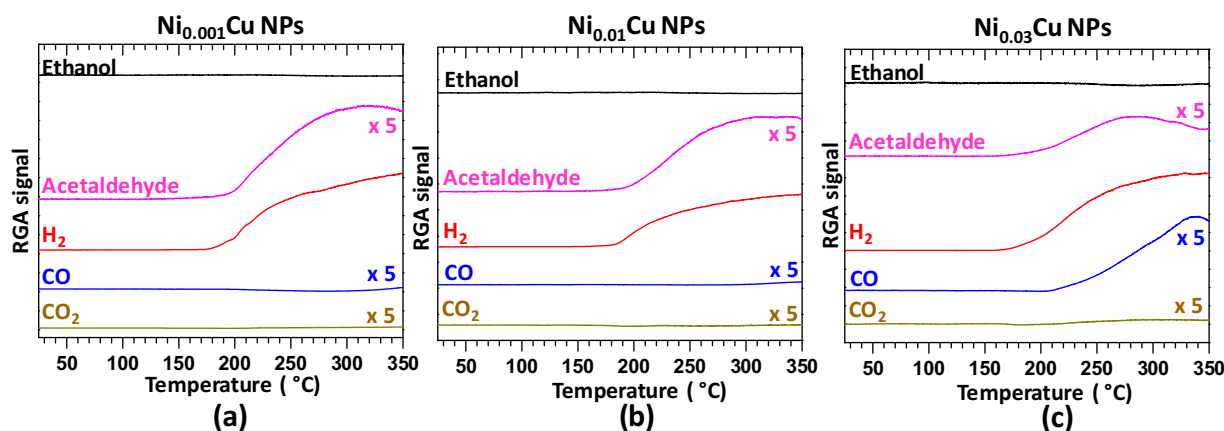
Fig. 6. TPSR of ethanol on (a) silica supported $Ni_{0.001}Cu$ NPs, (b) silica supported $Ni_{0.01}Cu$ NPs, and (c) silica supported $Ni_{0.03}Cu$ NPs. Reaction conditions: 100 mg catalyst, 6% ethanol balanced in He, He flow rate 10 mL/min.
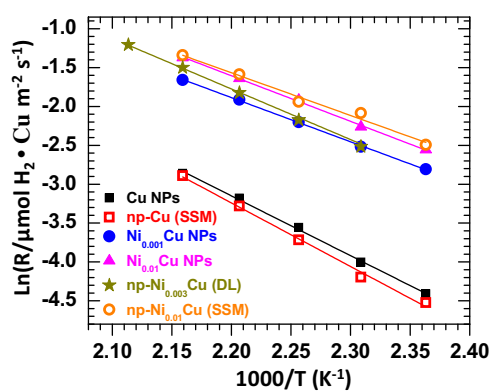

Fig. 7. Arrhenius-type plots of the reaction rate normalized by the surface area of Cu over monometallic Cu NPs and various highly dilute NiCu alloys used in the selective dehydrogenation of ethanol.

Table 3
List of the apparent activation energy of various highly dilute NiCu alloys determined from Fig. 7.

Samples	E_a (kJ/mol)
Cu NPs	70 ± 5
np-Cu (SSM)	73 ± 6
$Ni_{0.001}Cu$ NPs	49 ± 4
$Ni_{0.01}Cu$ NPs	47 ± 2
np-$Ni_{0.003}Cu$ (DL)	53 ± 6
np-$Ni_{0.01}Cu$ (SSM)	45 ± 4

type plots in Fig. 7 are shown in Table 3. The apparent activation energy determined for monometallic Cu NPs is 70 ± 5 kJ/mol and for np-Cu (SSM) it is 73 ± 6 kJ/mol, while for $Ni_{0.001}Cu$ NPs, $Ni_{0.01}Cu$ NPs, np-$Ni_{0.003}Cu$ (DL), and np-$Ni_{0.01}Cu$ (SSM) it is 49 ± 4 kJ/mol, 47 ± 2 kJ/mol, 53 ± 5 kJ/mol, and 45 ± 4 kJ/mol, respectively. Clearly, adding a small amount of Ni to Cu significantly decreases the apparent activation energy of the reaction, or in other words improves the reactivity of Cu. On the other hand, np-Cu (SSM) has similar apparent activation energy as supported Cu NPs. Furthermore, the apparent activation energy of np-Cu (DL) is also 70 ± 3 kJ/mol (not shown here), indicating similar catalytic activity of np-Cu with supported monometallic Cu NPs.

Fig. 8 shows stability tests of the silica supported monometallic Cu NPs, $Ni_{0.001}Cu$ NPs, and $Ni_{0.01}Cu$ NPs, and the unsupported np-$Ni_{0.01}Cu$ (SSM) in ethanol dehydrogenation reaction at 250 °C (a); stability tests of the silica supported monometallic Cu NPs, and $Ni_{0.01}Cu$ NPs at 300 °C (b). Clearly, for the supported monometallic

Cu NPs a quick deactivation is observed at the reaction temperature of 250 °C and 300 °C. The activity decreases approximately 25% after 8 h of reaction at 250 °C, while it decreases approximately 50% after 12 h of reaction at 300 °C. Note that no residual carbon was found in temperature programmed oxidation (TPO) measurements on the used Cu catalysts, indicating that carbon deposition is not the reason for the deactivation. Previous studies have reported that sintering of Cu causes the observed deactivation [1,7,14]. Interestingly, the Ni-containing supported NiCu NPs and unsupported np-NiCu (SSM) do not exhibit significant deactivation after 8 h in ethanol dehydrogenation reaction at 250 °C. Whereas, after 12 h reaction at 300 °C, the $Ni_{0.01}Cu$ NP shows only a very small drop of activity. Since the main cause of deactivation of Cu catalysts is reported to be sintering, it is likely that adding Ni to Cu can prevent the sintering of Cu at elevated temperatures. Furthermore, after normalized by the copper surface area, the H_2 formation rates on NiCu highly dilute alloys are significantly higher than that on monometallic Cu, showing the higher reactivity of NiCu alloy catalysts than Cu, which is in agreement with the apparent activation energies obtained from Fig. 7. Interestingly, the areal activities of $Ni_{0.001}Cu$ NPs and the nanoporous np-$Ni_{0.01}Cu$ (SSM) are similar, as shown in Fig. 8 (a). In our previous studies, we found that the Cu NPs prepared with the same protocol are single crystal NPs with a (111) surface [38], whereas, np-Cu based NiCu alloys have other crystal orientations presented, for example (110). Thus, the non-oxidative ethanol dehydrogenation reaction over NiCu highly dilute alloys appears to be surface-insensitive. However, since the surface concentration of Ni differs among the samples, additional mechanistic work is needed to determine the TOFs of the reaction over the NiCu catalysts.

Fig. 9 shows long-term stability tests of np-Cu (DL) and np-$Ni_{0.003}Cu$ (DL) in the ethanol dehydrogenation reaction at 250 °C for approximately 43 h. The ethanol conversion over np-Cu (DL) drops by $\sim$ 8% after the reaction for 43 h. Clearly, the stability of np-Cu (DL) is much better than the supported Cu NPs in Fig. 8. This could be due to the presence of Zn in the nanoporous Cu sample, which may improve the stability of Cu by preventing its sintering; or it may be due to the nanoporous structure of np-Cu (DL), which may have better structural stability against sintering. On the other hand, the ethanol conversion over np-$Ni_{0.003}Cu$ (DL) only decreases approximately 2% after the reaction for 43 h. Clearly, adding Ni to np-Cu (DL) can further improve the stability. Furthermore, although the same amounts of np-Cu (DL) and np-$Ni_{0.003}Cu$ (DL) were used, as well as identical reaction parameters were employed in the long-term stability tests, the ethanol conversion is much higher in the
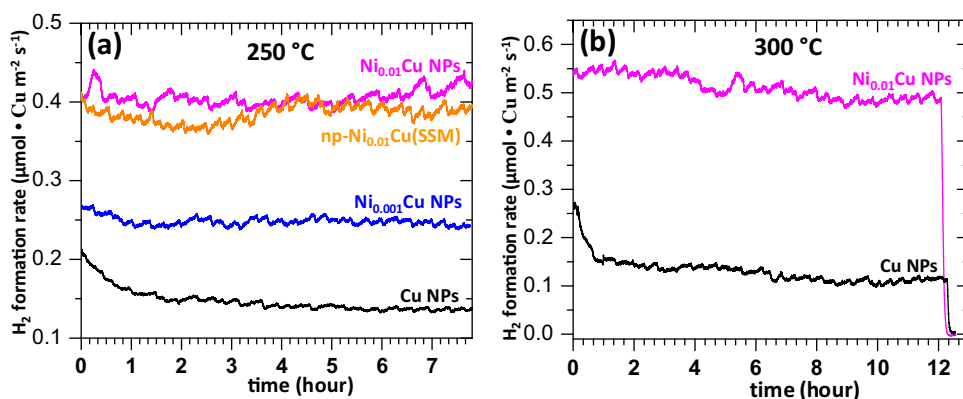
Fig. 8. Stability tests of silica supported monometallic Cu NPs, silica supported $Ni_{0.001}Cu$ NPs, silica supported $Ni_{0.01}Cu$ NPs, and np-$Ni_{0.01}Cu$ (SSM) in ethanol dehydrogenation reaction at 250 °C (a); stability tests of silica supported monometallic Cu NPs, and silica supported $Ni_{0.01}Cu$ NPs at 300 °C. The reaction rates are normalized by the surface area of Cu in each catalyst.
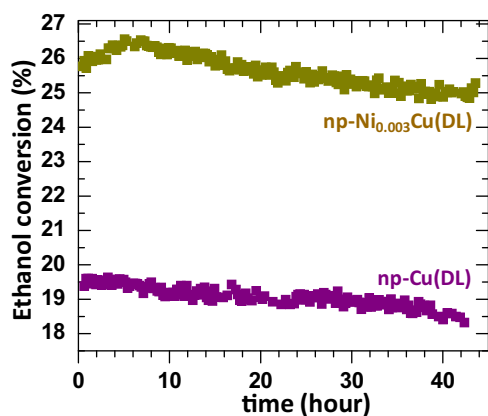

Fig. 9. Long-term stability tests of np-Cu (DL) and np-$Ni_{0.003}Cu$ (DL) in the ethanol dehydrogenation reaction at 250 °C for approximately 43 h. The same amount of catalysts (30 mg) was used.

case of np-$Ni_{0.003}Cu$ (DL), indicating that adding a small amount of Ni improves the activity of np-Cu (DL), similar to the case of Cu NPs.

Fig. 10 shows SEM images of np-Cu (DL) before and after ethanol dehydrogenation reaction at 250 °C for 60 h, (a) and (b); as well as SEM images of np-$Ni_{0.003}Cu$ (DL) before and after ethanol dehydrogenation reaction at 250 °C for 60 h, (c) and (d). The average ligament size of np-Cu (DL) before reaction is 165 ± 35 nm, whereas after reaction it is 335 ± 84 nm. Therefore, the ethanol dehydrogenation reaction leads to coarsening of np-Cu. On the other hand, the average ligament size of np-$Ni_{0.003}Cu$ (DL) before reaction is 192 ± 46 nm, and after reaction it is 198 ± 50 nm. Clearly, there is no coarsening of np-NiCu after the reaction, which is consistent with the stability tests shown in Fig. 9.

As discussed above, these highly dilute NiCu alloys are very active for the non-oxidative ethanol dehydrogenation reaction, with nearly 100% selectivity to acetaldehyde. The sample characterizations show that Ni atoms are highly dispersed in Cu. During the ethanol dehydrogenation reaction, part of Ni moves into in the subsurface region. Although Cu NPs have been reported to be active for this reaction, the quick deactivation of the catalyst remains an unresolved issue. As for supported monometallic Ni catalysts, a worse selectivity to acetaldehyde and a much quicker deactivation of the catalyst has been reported [59]. We found that adding a small amount of Ni to Cu, forming atomically dilute NiCu alloys, significantly improves the catalyst stability at 250 °C. Furthermore, adding a small amount of Ni to Cu can also dramatically enhance the activity of the catalysts. The apparent activation energy decreases

from ~70 kJ/mol over Cu to ~45 kJ/mol over the NiCu alloys. Thus, addition of Ni has also an electronic effect on Cu, which warrants further investigation.

Of note, the obtained apparent activation energies, ~70 kJ/mol over Cu/SiO_2 NPs and np-Cu, are in good agreement with values that have been reported on non-reducible oxide supported Cu NPs [11]; whereas, for Cu NPs supported on reducible oxides, the apparent activation energy is much smaller. Such differences could result from the different oxidation state of Cu, the different Cu dispersion, and the different metal-support interaction [11,60,61]. In the present study, by comparison of the apparent activation energy of the same type of catalysts with and without Ni, we show that the presence of a small amount of Ni in Cu can also significantly change the reactivity of the catalyst.

Bimetallic NiCu catalysts have been found to be active for the ethanol steam reforming reaction [62,63]. The reactivity and stability of bimetallic NiCu are much better than monometallic Cu catalysts. However, the presence of Ni islands causes the decomposition of ethanol, leading to the formation of CO, which is an undesired product [62,63]. A similar effect of Ni may be expected in the ethanol dehydrogenation reaction. However, we found that highly dispersed Ni in Cu does not cause the decomposition of ethanol to CO (except for higher Ni concentrations like the one shown in Fig. 6c). At the compositions employed here, Ni may be in the form of isolated atoms or atomically dispersed nanoclusters. Further work is warranted to discriminate between these structures, as they were shown to play a key role in improving both the activity and the stability of Cu in the ethanol dehydrogenation reaction.

4. Conclusions

In this work, we demonstrated that highly dilute NiCu alloys are very active for the non-oxidative dehydrogenation of ethanol to acetaldehyde and hydrogen under realistic conditions with nearly 100% selectivity. Adding a small amount of Ni to the Cu surface does not only significantly increase the reactivity of copper, but also greatly improves its stability. Our data show that the presence of Ni atoms in the Cu surface may not only stabilize the morphology of Cu catalysts but also have a direct effect on the reaction mechanism. This work opens a new route for the use of highly dilute alloys for alcohol dehydrogenation reactions. Furthermore, the comparison of the catalytic performance of highly dilute alloy NPs with nanoporous materials is useful to guide the design of novel mesoporous catalyst architectures for selective dehydrogenation or oxidation reactions.
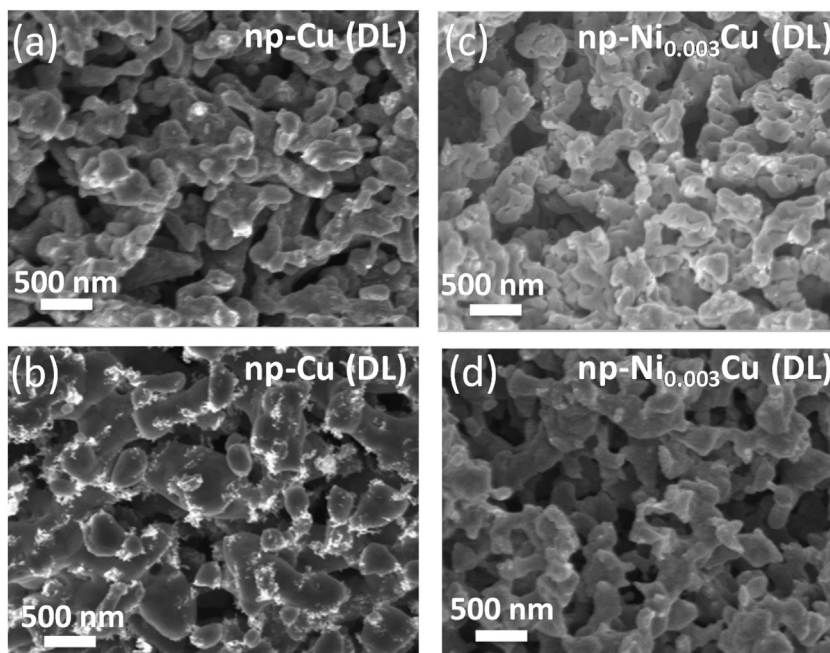
Fig. 10. (a) SEM images of np-Cu (DL) before reaction; (b): np-Cu (DL) after ethanol dehydrogenation reaction at 250 °C for 60 h; (c): np-Ni$_{0.003}$Cu (DL) before reaction; (d): np-Ni$_{0.003}$Cu (DL) after ethanol dehydrogenation reaction at 250 °C for 60 h.

Acknowledgements

References

[1] M. Eckert, G. Fleischmann, R. Jira, H.M. Bolt, K. Golka, Ullmann's Encyclopedia of Industrial Chemistry, Wiley-VCH Verlag GmbH & Co. KGaA, Weinheim, Germany, 2007.
[2] H.J. Hagemeyer, Acetaldehyde Kirk Othmer Encyclopedia of Chemical Technology, John Wiley & Sons, Inc, Hoboken, NJ, USA, 2002.
[3] Y.J. Guan, E.J.M. Hensen, Appl. Catal. A-Gen. 361 (2009) 49–56.
[4] F.W. Chang, H.C. Yang, L.S. Roselin, W.Y. Kuo, Appl. Catal. A-Gen. 304 (2006) 30–39.
[5] M.C. Sanchez-Sanchez, R.M.N. Yerga, D.I. Kondarides, X.E. Verykios, J.L.G. Fierro, J. Phys. Chem. A 114 (2010) 3873–3882.
[6] J.M. Sun, A.M. Karim, D.H. Mei, M. Engelhard, X.H. Bao, Y. Wang, Appl. Catal. B-Environ. 162 (2015) 141–148.
[7] Y.J. Tu, Y.W. Chen, Ind. Eng. Chem. Res. 40 (2001) 5889–5893.
[8] M. Besson, P. Gallezot, Catal. Today 57 (2000) 127–141.
[9] E.A. Redina, A.A. Greish, I.V. Mishin, G.I. Kapustin, O.P. Tkachenko, O.A. Kirichenko, L.M. Kustov, Catal. Today 241 (2015) 246–254.
[10] I.C. Freitas, S. Damyanova, D.C. Oliveira, C.M.P. Marques, J.M.C. Bueno, J. Mol. Catal. A-Chem. 381 (2014) 26–37.
[11] W.H. Cassinelli, L. Martins, A.R. Passos, S.H. Pulcinelli, A. Rochet, V. Briois, C.V. Santilli, ChemCatChem 7 (2015) 1668–1677.
[12] W.H. Cassinelli, L. Martins, M. Magnani, S.H. Pulcinelli, V. Briois, C.V. Santilli, RSC Adv. 6 (2016) 20453–20457.
[13] S.W. Colley, J. Tabatabaei, K.C. Waugh, M.A. Wood, J. Catal. 236 (2005) 21–33.
[14] F.W. Chang, W.Y. Kuo, K.C. Lee, Appl. Catal. A-Gen. 246 (2003) 253–264.
[15] Y.J. Tu, Y.W. Chen, C.P. Li, J. Mol. Catal. 89 (1994) 179–190.
[16] E. Santacesaria, G. Carotenuto, R. Tesser, M. Di Serio, Chem. Eng. J. 179 (2012) 209–220.
[17] C.Y. Wang, G. Garbarino, L.F. Allard, F. Wilson, G. Busca, M. Flytzani-Stephanopoulos, ACS Catal. 6 (2016) 210–218.
[18] A. Gazsi, A. Koos, T. Bansagi, F. Solymosi, Catal. Today 160 (2011) 70–78.
[19] A. Ciftci, D.A.J.M. Ligthart, P. Pastorino, E.J.M. Hensen, Appl. Catal. B-Environ. 130 (2013) 325–335.
[20] M. Flytzani-Stephanopoulos, B.C. Gates, Annu. Rev. Chem. Biomol. Eng. 3 (2012) 545–574.
[21] C.Y. Wang, M. Yang, M. Flytzani-Stephanopoulos, AIChE J. 62 (2016) 429–439.
[22] M. Yang, J.L. Liu, S. Lee, B. Zugic, J. Huang, L.F. Allard, M. Flytzani-Stephanopoulos, J. Am. Chem. Soc. 137 (2015) 3470–3473.
[23] M. Yang, S. Li, Y. Wang, J.A. Herron, Y. Xu, L.F. Allard, S. Lee, J. Huang, M. Mavrikakis, M. Flytzani-Stephanopoulos, Science 346 (2014) 1498–1501.
[24] Y.P. Zhai, D. Pierre, R. Si, W.L. Deng, P. Ferrin, A.U. Nilekar, G.W. Peng, J.A. Herron, D.C. Bell, H. Saltsburg, M. Mavrikakis, M. Flytzani-Stephanopoulos, Science 329 (2010) 1633–1636.
[25] N. El Kolli, L. Delannoy, C. Louis, J. Catal. 297 (2013) 79–92.
[26] G.X. Pei, X.Y. Liu, A.Q. Wang, L. Li, Y.Q. Huang, T. Zhang, J.W. Lee, B.W.L. Jang, C.Y. Mou, New J. Chem. 38 (2014) 2043–2051.
[27] A.J. McCue, R.T. Baker, J.A. Anderson, Faraday Discuss. 188 (2016) 499–523.
[28] B. Pongthawornsakun, S. Fujita, M. Arai, O. Mekasuwandumrong, J. Panpranot, Appl. Catal. A-Gen. 467 (2013) 132–141.
[29] P. Dash, N.A. Dehm, R.W.J. Scott, J. Mol. Catal. A-Chem. 286 (2008) 114–119.
[30] B. Zugic, S. Karakalos, K.J. Stowers, M.M. Biener, J. Biener, R.J. Madix, C.M. Friend, ACS Catal. 6 (2016) 1833–1839.
[31] A. Wittstock, V. Zielasek, J. Biener, C.M. Friend, M. Baumer, Science 327 (2010) 319–322.
[32] B.J. Xu, C.G.F. Siler, R.J. Madix, C.M. Friend, Chem.-Eur. J. 20 (2014) 4646–4652.
[33] L.C. Wang, K.J. Stowers, B. Zugic, M.L. Personick, M.M. Biener, J. Biener, C.M. Friend, R.J. Madix, J. Catal. 329 (2015) 78–86.
[34] K. Suzuki, T. Yamaguchi, K. Matsushita, C. Iitsuka, J. Miura, T. Akaogi, H. Ishida, ACS Catal. 3 (2013) 1845–1849.
[35] J. Greeley, M. Mavrikakis, J. Phys. Chem. B 109 (2005) 3460–3471.
[36] J.L. Liu, F.R. Lucci, M. Yang, S. Lee, M.D. Marcinkowski, A.J. Therrien, C.T. Williams, E.C.H. Sykes, M. Flytzani-Stephanopoulos, J. Am. Chem. Soc. 138 (2016) 6396–6399.
[37] F.R. Lucci, J.L. Liu, M.D. Marcinkowski, M. Yang, L.F. Allard, M. Flytzani-Stephanopoulos, E.C.H. Sykes, Nat. Commun. 6 (2015).
[38] M.B. Boucher, B. Zugic, G. Cladaras, J. Kammert, M.D. Marcinkowski, T.J. Lawton, E.C.H. Sykes, M. Flytzani-Stephanopoulos, Phys. Chem. Chem. Phys. 15 (2013) 12187–12196.
[39] M.B. Boucher, M.D. Marcinkowski, M.L. Liriano, C.J. Murphy, E.A. Lewis, A.D. Jewell, M.F.G. Mattera, G. Kyriakou, M. Flytzani-Stephanopoulos, E.C.H. Sykes, ACS Nano. 7 (2013) 6181–6187.
[40] J. Shan, F.R. Lucci, J. Liu, M. El-Soda, M.D. Marcinkowski, L.F. Allard, E.C.H. Sykes, M. Flytzani-Stephanopoulos, Surf. Sci. 650 (2016) 121–129.
[41] Z.Y. Li, C.H. Han, J.Y. Shen, J. Mater. Sci. 41 (2006) 3473–3480.
[42] A. Serov, K. Artyushkova, E. Niangar, C.M. Wang, N. Dale, F. Jaouen, M.T. Sougrati, Q.Y. Jia, S. Mukerjee, P. Atanassov, Nano Energy 16 (2015) 293–300.
[43] T. Tachiwaki, M. Suzuki, H. Okajima, S. Koizumi, T. Ito, A. Hiraki, Appl. Surf. Sci. 70–71 (1993) 751–754.
[44] N.A. Dhas, C.P. Raj, A. Gedanken, Chem. Mater. 10 (1998) 1446–1452.
[45] S. Jeong, K. Woo, D. Kim, S. Lim, J.S. Kim, H. Shin, Y.N. Xia, J. Moon, Adv. Funct. Mater. 18 (2008) 679–686.

[46] Z.L. Zhang, Y.J. Ji, J. Li, Z.Y. Zhong, F.B. Su, RSC Adv. 5 (2015) 54364–54371.
[47] Y. Yoshida, K. Uto, M. Hattori, M. Tsuji, CrystEngComm 16 (2014) 5672–5680.
[48] S.J. Pennycook, Adv. Imag. Electron. Phys. 123 (2002) 173–206.
[49] G.C. Bond, S.N. Namijo, J. Catal. 118 (1989) 507–510.
[50] A.P. Grosvenor, M.C. Biesinger, R.S. Smart, N.S. McIntyre, Surf. Sci. 600 (2006) 1771–1779.
[51] J.J. Shan, W.X. Huang, L. Nguyen, Y. Yu, S.R. Zhang, Y.Y. Li, A.I. Frenkel, F. Tao, Langmuir 30 (2014) 8558–8569.
[52] S. D'Addato, V. Grillo, S. Altieri, R. Tondi, S. Valeri, S. Frabboni, J. Phys.-Condens. Mater. 23 (2011).
[53] P. Prieto, V. Nistor, K. Nouneh, M. Oyama, M. Abd-Lefdil, R. Diaz, Appl. Surf. Sci. 258 (2012) 8807–8813.
[54] M. Komarneni, J. Shan, U. Burghaus, J. Phys. Chem. C 115 (2011) 16590–16597.
[55] N.D. Subramanian, C.S.S.R. Kumar, K. Watanabe, P. Fischer, R. Tanaka, J.J. Spivey, Catal. Sci. Technol. 2 (2012) 621–631.
[56] S.F. Moya, R.L. Martins, M. Schmal, Appl. Catal. A-Gen. 396 (2011) 159–169.
[57] G. Poncelet, M.A. Centeno, R. Molina, Appl. Catal. A.-Gen. 288 (2005) 232–242.
[58] J.A. Anderson, M.T. Rodrigo, L. Daza, S. Mendioroz, Langmuir 9 (1993) 2485–2490.
[59] A. Neramittagapong, W. Attaphaiboon, S. Neramittagapong, Chiang Mai J. Sci. 35 (2008) 171–177.
[60] A.G. Sato, D.P. Volanti, D.M. Meira, S. Damyanova, E. Longo, J.M.C. Bueno, J. Catal. 307 (2013) 1–17.
[61] K. Sun, M.H. Zhang, L.C. Wang, Chem. Phys. Lett. 585 (2013) 89–94.
[62] L.C. Chen, S.D. Lin, Appl. Catal. B-Environ. 148 (2014) 509–519.
[63] F. Wang, Y. Li, W.J. Cai, E.S. Zhan, X.L. Mu, W.J. Shen, Catal. Today 146 (2009) 31–36.